Effect of pressure on single-chain magnets with repeating units of the Mn^{III}-Ni^{II}-Mn^{III} trimer

Masaki Mito,[1,2,*] Hiroyuki Deguchi,[1,2] Takayuki Tajiri,[1] Seishi Takagi,[1] Masahiro Yamashita,[2,3] and Hitoshi Miyasaka[2,4,5]
[1]*Faculty of Engineering, Kyushu Institute of Technology, Kitakyushu 804-8550, Japan*
[2]*CREST, Japan Science and Technology Agency (JST), Saitama 332-0012, Japan*
[3]*Department of Chemistry, Tohoku University, Sendai 980-8578, Japan*
[4]*Department of Chemistry, Tokyo Metropolitan University, Tokyo 192-0397, Japan*
[5]*PRESTO, Japan Science and Technology Agency (JST), Saitama 332-0012, Japan*
(Received 21 June 2005; published 24 October 2005)

The single-chain magnet (SCM) system $[Mn_2(saltmen)_2Ni(pao)_2(L)_2](A)_2$ (L: intrachain attaching ligand of Ni^{II} ion; A^{-1}: interchain counteranion) is a ferromagnetic one-dimensional network system with repeating units of the Mn^{III}-Ni^{II}-Mn^{III} trimer which itself behaves as a single-molecule magnet with an $S=3$ spin ground state and negative uniaxial single-ion anisotropy (D) parallel to the bridging direction. The slow relaxation of the magnetic moment in this SCM system originates in an energy barrier for spin reversal (ΔE), which is closely related to the ferromagnetic interaction between the trimers (J_{trimer}) as well as to the D of the trimer. We have investigated the effects of pressure on three compounds representative of the above SCM family through ac susceptibility measurements under hydrostatic pressures up to $P=13.5$ kbar and crystal structural analysis experiments up to $P=20.0$ kbar, and have observed a pronounced enlargement of ΔE when J was artificially increased. The application of hydrostatic pressure brought about the systematic enhancement of ΔE (a maximum increase of 10% within the pressure region of the experiments). The pressure dependence of ΔE varied according to the kind of attaching ligand L involved and the intrachain structure, and we have experimentally found that isotropic lattice shrinkage is desirable if a continuous increase of ΔE in this system is aimed at.

DOI: 10.1103/PhysRevB.72.144421 PACS number(s): 75.50.Xx, 75.40.Gb, 81.40.Vw

I. INTRODUCTION

The creation of new nanomagnets based on the low-dimensional magnetic systems is a challenging subject in the material science today, from the viewpoints of both fundamental research and applications such as information storage or quantum computation. The strategy for creating nanomagnets is to utilize the metastable magnetic state without long-range order and fundamentally associated with the presence of a high-spin ground state and magnetic anisotropy given by a nanosized particle. With a focus on zero-dimensional (0D) and one-dimensional (1D) systems, many molecule-based magnets have been extensively explored to date in the hope of creating high-bit memory media.

A well-known example of the 0D system is cluster magnets such as the dodecanuclear manganese complex Mn_{12} (Ref. 1) and the octanuclear iron complex Fe_8,[2] referred to as single-molecule magnets (SMMs), and they have been attracting the attention of many material scientists. In SMMs, the magnetic ground state of large spin quantum number (S) and negative uniaxial anisotropy ($D<0$; D is defined as the zero-field splitting parameter) bring about a finite energy barrier (ΔE) for spin reversal between the up-spin and down-spin states, and the barrier height is roughly estimated to be $|D|S^2$ for integer spin and $|D|(S^2-1/4)$ for half-integer spin. The energy barrier is thermally activated and restricts the reversal of the magnetic moment below the so-called "blocking temperature" (T_B). The global magnetization decays with the relaxation time (τ) inherent to the material, which increases exponentially with decreasing temperature. The relaxation time might extend to years below T_B. Thus, in this system, each cluster can behave like a magnet, with remnant magnetic moment over a finite time scale.

In the 1D system as well as 0D (SMMs system), there is no long-range order independently of spin symmetry, as proved by Onsager's exact solution.[3] As for the 1D system, in 1963, Glauber famously proposed a model of slow relaxation of the magnetic moment in the Ising ferromagnetic spin system.[4] In his model, the relaxation time depends on the correlation length. Phenomenologically, however, magnetic relaxation of the Glauber type has not been observed until recently, and the relaxation process characterized by Glauber's model has been successively observed at length in the following two 1D compounds in 2001 to 2002; (1) a helical 1D compound $[Co^{II}(hfac)_2(NITPhOMe)]$ (hfac=hexafluoroacetylacetonate and NITPhOMe=4′-methoxy-phenyl-4,4,5,5-tetramethylimidazoline-1-oxyl-3-oxide),[5,6] and (2) a heterometallic chain with repeating units of the Mn^{III}-N^{II}-Mn^{III} trimer, $[Mn_2(saltmen)_2Ni(pao)_2(py)_2](ClO_4)_2$ ($saltmen^{2-}$=*N*,*N*′-(1,1,2,2-tetramethylethylene) bis (salicylideneiminate) and pao^-=pyridine-2-aldoximate).[7–9] In the above compounds, the slow relaxation of the magnetic moment is not caused by isolated anisotropic entities such as SMMs, which would individually relax slowly, but by the introduction of a magnetic correlation between quickly relaxing units. By analogy to SMMs, the above type has been called single-chain magnet (SCM). This SCM system has two such important characteristics: a negative D vector, which locks the direction of the spins along the chain, and a ferromagnetic interaction (J), which yields short-range ordering at low temperatures. The energy barrier ΔE should be a function of J as well as D,[8,9] and each chain can be regarded as a magnet within a finite time scale.

The first helical 1D compound mentioned, discovered by Caneschi *et al.*, comprises alternately arranged anisotropic

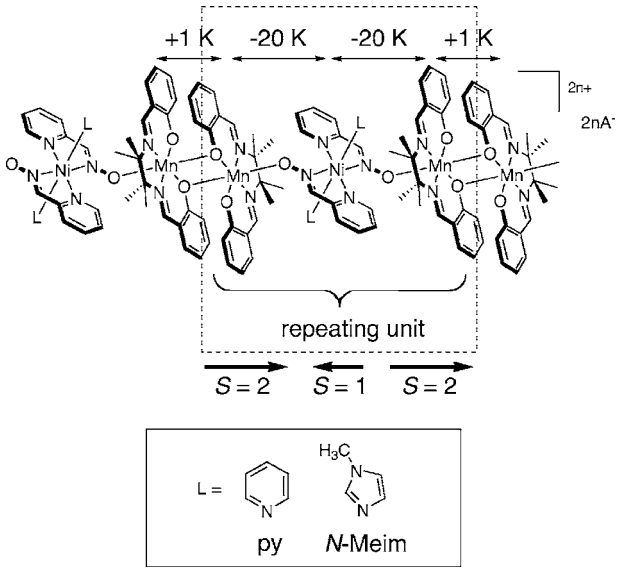

FIG. 1. Chain structure of the $[Mn_2(saltmen)_2Ni(pao)_2(L)_2]\times(A)_2$ family. L stands for an intrachain attaching ligand on Ni^{II} ion, and A^{-1} stand for an interchain counteranion. (1): L =pyridine (py), $A^-=ClO_4^-$; (2): L=py, $A^-=ReO_4^-$; and (3): L=*N*-methylimidazole (*N*-Meim), $A^-=ClO_4^-$.

Co^{II} ion and the isotropic organic radical NITPhOMe: the 1D array has a helical structure arising from the trigonal crystallographic lattice. The effective 1/2 spin of the Co^{II} ions and the 1/2 spin of the radical are characterized by different g-values ($g_{Co}=7.4$, $g_{rad}=2.0$), and in consequence the chain behaves as a 1D ferromagnetic-type SCM because of the noncompensation of the magnetic moments.[5,6] In particular, an Arrhénius-type slow relaxation with a $\Delta E/k_B$ value of 152 K has been observed (ten decades of relaxation time), and it has been reported that the behavior is consistent with the extended Glauber's model considering helical geometrical factors.[6] The helical chain structure does not allow the hard plane orthogonal to the trigonal axis, and a pictorial representation may be necessary to understand the helical spin texture.

On the other hand, the second 1D compound mentioned, discovered by Clérac and Miyasaka *et al.*, has an ideal chain structure with an easy axis parallel to the unique chain orientation as seen in Fig. 1, and can be regarded as an $S=3$ Heisenberg ferromagnetic chain comprising [Mn^{III}-Ni^{II}-Mn^{III}] trimers with a negative D-vector parallel to the chain. In fact, the trimer itself behaves as a SMM with a $\Delta E/k_B$ value of 18 K.[10] The anisotropy originates from the Jahn-Teller distortion of the Mn^{III} ion, and the dynamic properties of the SCM system are accounted for by Arrhénius's law.[7,8] In this sense, the second is a simplified SCM system. A detailed explanation of the structure of this family will be given in the next section. The Hamiltonian of the second SCM compound is yielded by the Heisenberg-type spin operator ($\boldsymbol{S}_i$) and the negative single-ion anisotropy parameter D, as follows:

$$H=-2J\sum_i \boldsymbol{S}_i\cdot\boldsymbol{S}_{i+1}+D\sum_i (S_i^z)^2, \quad (1)$$

where the z axis is the chain direction and J is the ferromagnetic exchange constant between the spin units of $S=3$.[9] In the systematic study by Miyasaka *et al.*,[8] it has been experimentally pointed out that the ΔE of this system should be a function of J and D in the range of $|D|>4J/3$, as follows:

$$\Delta E=(8J+|D|)S^2. \quad (2)$$

From the viewpoint of the materials design of molecular nanomagnets, SCMs may have greater potentiality than SMMs, since the intrinsic properties of SCMs can be controlled through the J as well as the D. As for controlling the J, there is still room for improvement at the stage of materials synthesis, and further chemical modification of the one-dimensional structure will open new attractive avenues of research. Thus the material scientists are encouraged to manipulate the structure with a view to giving the material specific characteristics. Our strategy is to attempt a delicate control of the material by subjecting it to external stress, *i.e., pressure*, and to optimally fine-tune the correlation between magnetism and structure in model compounds. Two important parameters, J and D, are assumed to be tuned when orbital overlapping and the ligand environment are modified *effectively and continuously* under pressure, but the change in J is assumed to predominate over that in D. A previous study of a Mn_{12}-acetate under pressure has shown that the maximum change in $|D|$ is about +3.5% at $P=10$ kbar.[11] We herein present the effects of pressure on three model compounds belonging to the $[Mn_2(saltmen)_2Ni(pao)_2(L)_2](A)_2$ family, where L and A^{-1} are an intrachain attaching ligand on Ni^{II} ion and an interchain counteranion, respectively. Through this study, we would like to demonstrate the possibility of controlling materials using pressure, and of applying this method in the field of molecule-based functional magnets. The resultant experimental knowledge of the magneto-structural correlation via these pressure experiments would be fed back into the field of materials fabrication as very important information for novel molecular design.

II. EXPERIMENT

Three model compounds belonging to the $[Mn_2(saltmen)_2Ni(pao)_2(L)_2](A)_2$ family, (1) L=pyridine (py) and $A^-=ClO_4^-$, (2) L=py and $A^-=ReO_4^-$, and (3) L =*N*-methylimidazole (*N*-Meim) and $A^-=ClO_4^-$, have been synthesized according to the procedure described elsewhere.[7,8] Figure 1 shows the chain structure of the $[Mn_2(saltmen)_2Ni(pao)_2(L)_2](A)_2$ family, and the chain runs along the ⟨101⟩ direction. The crystals for compounds (1)–(3) were confirmed to crystallize as monoclinic $C2/c$ space group; the lattice parameters are shown in Table I.[8] The geometry of the Ni^{II} ion, the center of the repeating unit with an inversion center, is a slightly distorted octahedron. The bonding distance in Ni-N along the chain is smaller than that in Ni-N outside the chain. The bonding angles in Ni-N-O and N-O-Mn along the chain are far from a right angle (for example, Ni-N-O=123.9(3)° and N-O-Mn=131.8(3)° in the

TABLE I. Lattice parameters for compounds (1)–(3) in monoclinic space group $C2/c$ (Ref. 8).

	(1)	(2)	(3)
a(Å)	21.140	20.860	21.029
b(Å)	15.975	16.010	15.978
c(Å)	18.621	18.732	18.630
β(°)	98.059	98.115	98.063
V(Å^3)	6226.5	6193.3	6197.9

case of compound (1)[7]) and, consequently, an antiferromagnetic superexchange interaction ($J_{\text{Mn-Ni}}$) of about −20 K works between the Ni^{II} ion and the neighboring Mn^{III} ions, via the -ON- bond. On the other hand, the Mn sites assume a sixfold coordination geometry with a Jahn-Teller distortion, and the apical position of the $[Mn(saltmen)]^+$ is occupied by a phenolate oxygen arising from the neighboring $[Mn(saltmen)]^+$ moiety, in addition to the coordination with -ON- from the Ni^{II} moiety. The bonding angles in Mn-O-Mn and O-Mn-O on the coupling plane of $[Mn(saltmen)_2]$ dimeric moieties are almost rectangular (for example, Mn-O-Mn=98.9° and O-Mn-O=81.1° in the case of compound (1)[7]) and a ferromagnetic interaction (J_{trimer}) of about 1 K works between nearest neighboring [Mn^{III}-Ni^{II}-Mn^{III}] trimers via the almost orthogonal Mn-O-Mn bond ($J_{\text{Mn-Mn}}$ is about 2 K). Systematical study of Mn^{III} dimeric compounds in this family has confirmed that the magnitude of $J_{\text{Mn-Mn}}$ linearly depends on the bond length in Mn-O.[12] Furthermore, the elongation of the O-Mn-O bonds along the chain brings about the Mn^{III} Jahn-Teller distortion,[8] resulting in the appearance of a negative D vector of about −2.5 K parallel to the chain.[9] The existence of effective counteranion (A^-) can separate the chains markedly leaving minimum nearest interchain intermetallic distances such as 10.39 Å for compound (1),[7] 10.30 Å for compound (2)[8] and 10.36 Å for compound (3),[8] and there is no significant inter-chain π-π overlap between the aromatic rings. The interchain intermetallic distances hardly depend on the size of the counteranions. Thus, because at low temperatures the [Mn^{III}-Ni^{II}-Mn^{III}] trimer is considered to be an effective $S=3(=+2-1+2)$ unit, a heterometallic chain comprised of repeating units of [-$(O)_2$-Mn-ON-Ni-NO-Mn-] can be theoretically treated as an $S=3$ Heisenberg ferromagnetic chain with negative single-ion anisotropy. The essential magnetic properties of this system at ambient pressure are almost independent of the kinds of L and A^- involved. For reference, the data for $J_{\text{Mn-Ni}}$, J_{trimer}, and ΔE for compounds (1)–(3) at ambient pressure are listed in Table II.[8] In the present study, two kinds of L, py and *N*-Meim, were considered. Because that the volume of *N*-Meim is larger than that of py, we think that compound (3) with L=*N*-Meim has the densest chain structure among the three compounds. Through some counteranions, each chain is located with the sliding of a half period along the chain: The Mn^{III}-Mn^{III} dimer of a chain has the closest intermetallic contact with the Ni^{II} ion of the nearest neighboring chain. Thus, as for the interchain package, the structure in compound (3) is also the densest among the three, and consequently, possibly producing the minuscule void space only in the $[Mn_2(saltmen)_2]$ dimeric moieties.

TABLE II. $J_{\text{Mn-Ni}}/k_B$, J_{trimer}/k_B, and $\Delta E/k_B$ for compounds (1)–(3) (Ref. 8).

	(1)	(2)	(3)
$J_{\text{Mn-Ni}}/k_B$ (K)	−20.8	−21.2	−22.2
J_{trimer}/k_B (K)	0.70	0.84	0.76
$\Delta E/k_B$ (K)	72.0	72.6	70.9

The ac susceptibility measurements with an ac-field amplitude of 2 Oe at frequencies (f's) from 1.0 to 500 Hz were performed in the temperature region from 1.8 to 8.0 K, using a superconducting quantum interference device (SQUID) magnetometer (Quantum Design MPMS-5S) with an ac option. Pressure was attained using a piston-cylinder type of pressure cell (CR-PSC-KY05-1, Kyowa-Seisakusho Co., Ltd.), inserted into the SQUID magnetometer. The inner and outer diameters of the above pressure cell are 2.6 and 8.6 mm, respectively, and pressures up to 16.5 kbar can be applied at liquid-helium temperature. The main parts of the pressure cell such as the cylinder, locking nuts, etc., are made of nonmagnetic CuBe, and the pistons for transmitting the load to the sample are made of zirconia (ZrO_2). In order to apply pressure effectively, the sample was held inside the teflon cell with the aid of a pressure-transmitting medium, Apiezon-J grease, and a small amount of metallic superconductor lead. The pressures at liquid-helium temperature were estimated based on the shift in the superconducting transition temperature of the lead.[13]

Powder x-ray diffraction pattern analyses were carried out in the pressure region up to 20 kbar at room temperatures, using a synchrotron radiation x-ray powder diffractometer with a cylindrical imaging plate at the photon factory (PF) of the Institute of Materials Structure Science, the High Energy Accelerator Research Organization (KEK).[14] The wavelength of the incident x-ray was 0.6897(7 Å). Pressure was induced with a diamond-anvil cell (DAC), consisting of diamonds with flat tips of 0.6 mm in diameter and a CuBe gasket of 200 μm in thickness. The pressures were calibrated by the ruby fluorescence method.[15] In the sample cavity with a diameter of 0.2 mm, located in the center of the gasket, the powdered sample and a few ruby crystals were inserted with the aid of a pressure-transmitting medium, fluorine oil (FC77). The quality of the Debye-Scherrer ring was insufficient to perform the Rietveld analysis due to the nonhomogeneity of the powder size. The lattice parameters under pressure were estimated based on an analysis of the positions of some distinguishable diffraction peaks.

III. EXPERIMENTAL RESULTS

A. ac magnetic susceptibility

In compound (1), the frequency dependences of χ' and χ'' (defined as the in-phase and out-of-phase components of the ac susceptibility, respectively) for the three representative pressures are shown in Figs. 2 and 3. The frequency depen-

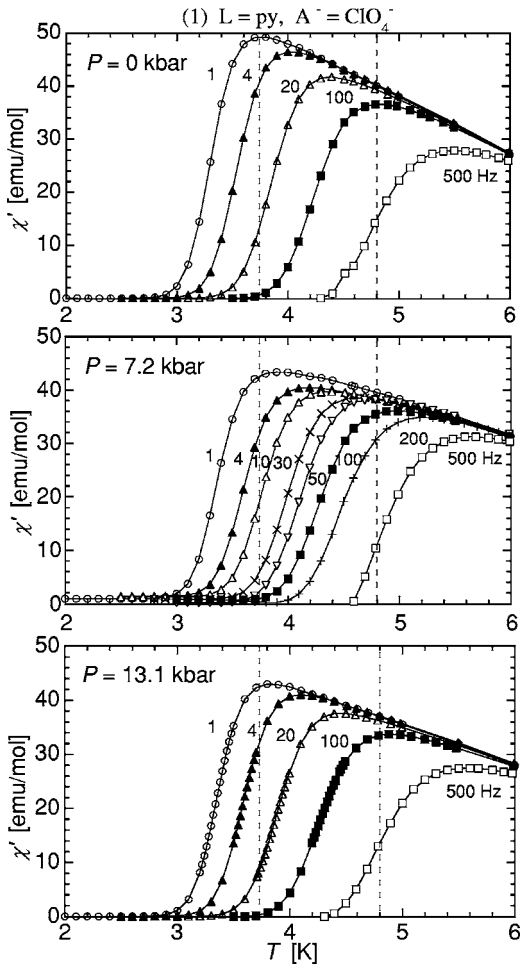

FIG. 2. Frequency dependence of the in-phase ac susceptibility (χ') on (1) (L=py, A^-=ClO_4^-) at P=0, 7.2, and 13.1 kbar. The broken lines represent the peak position for f=1 and 100 Hz at ambient pressure and play the role of guide for the eye to see the signal shift.

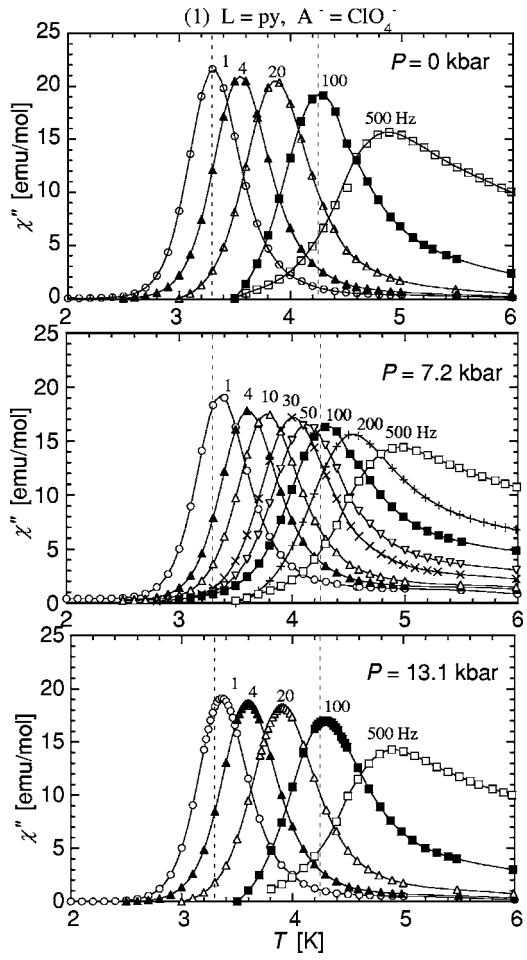

FIG. 3. Frequency dependence of out-of-phase ac susceptibility (χ') on (1) (L=py, A^-=ClO_4^-) at P=0, 7.2, and 13.1 kbar. The broken lines represent the peak position for f=1 and 100 Hz at ambient pressure and play the role of guide for the eye to see the signal shift.

dences of χ'' under pressure for compounds (2) and (3) are shown in Figs. 4 and 5, respectively. The pressure dependence of the blocking temperature (T_B) at f=1 Hz, the lowest frequency in the present experiments, for all compounds are shown in Fig. 6. Figure 7 shows the Arrhénius plots for the frequency dependence of T_B under pressure for all compounds, and the pressure dependences of ΔE estimated from the slopes are summarized in Fig. 8.

1. L=py, A^-=ClO_4^-

Figures 2 and 3 show the frequency dependence of χ' and χ'' on (1) (L=py, A^-=ClO_4^-) for P=0, 7.2, and 13.1 kbar, from among some measurements up to P=13.1 kbar. The data at ambient pressure in the frequency range up to 500 Hz show that a magnetic anomaly appears due to the magnetic freezing in the temperature region below 6.0 K. This anomaly shifts toward higher temperatures with increasing frequency, showing the typical behavior of critical slowing-down. Next, we compared the results under pressure with that at ambient pressure. For P=7.2 and 13.1 kbar, the temperature dependence of both χ' and χ'' at each frequency was similar to that at ambient pressure, and it was observed that the characteristics of SCMs were stable under pressure. However, attentive observation made us notice that pressurization led the shift of the frequency dependence for a series of anomalies toward higher temperatures. *The "frozen" magnetic state became more stable under pressure*. Keeping in mind that the temperature with the maximum of χ'' is defined as T_B at each frequency, we were able to determine in detail the pressure dependence of T_B at the lowest frequency, f =1 Hz, as shown in Fig. 6. Here, we stress that there is a systematic change in T_B, as follows. Below 7 kbar, T_B is enhanced with increasing pressure and, at around P=7 kbar, it begins to show a tendency toward saturation. Contrary to our excessive expectations, the maximum enhancement was 0.06 K at the highest pressure, P=13.1 kbar. However, it should be mentioned that a systematic change in the blocking phenomenon due to external stress has been clearly observed.

The frequency dependence of T_B under pressure for compound (1) was analyzed using an Arrhénius plot, as shown in Fig. 7. In the above mentioned report of Clérac and Miyasaka *et al.*, the frequency dependence was discussed on the

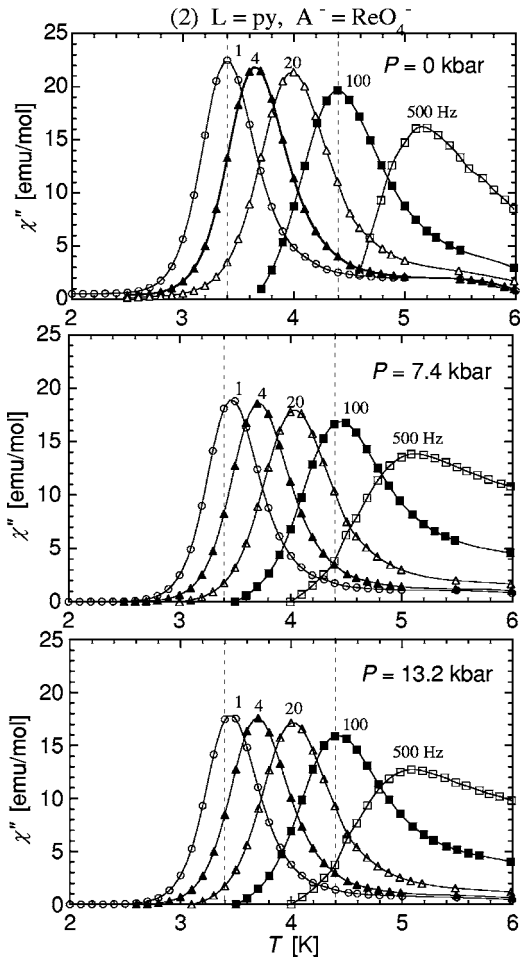

FIG. 4. Frequency dependence of out-of-phase ac susceptibility (χ') on (2) (L=py, A^-=ReO_4^-) at P=0, 7.4, and 13.2 kbar. The broken lines represent the peak position for f=1 and 100 Hz at ambient pressure and play the role of guide for the eye to see the signal shift.

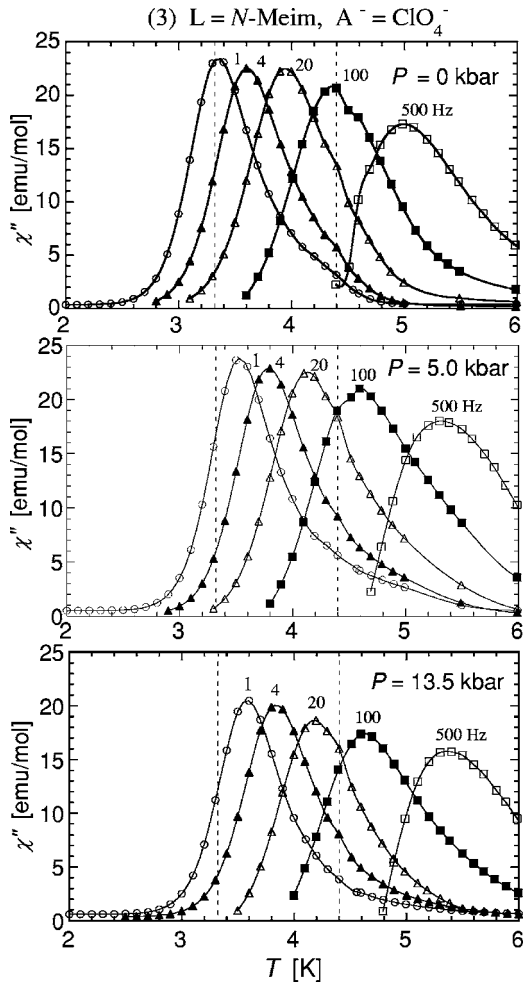

FIG. 5. Frequency dependence of out-of-phase ac susceptibility (χ') on (3) (L=*N*-Meim, A^-=ClO_4^-) at P=0, 5.0, and 13.5 kbar. The broken lines represent the peak position for f=1 and 100 Hz at ambient pressure and play the role of guide for the eye to see the signal shift.

assumption that the thermal variation of τ follows a thermal activation type as

$$\tau(T) = \tau_0 \exp(\Delta E/k_B T), \tag{3}$$

where τ_0 is a preexponential factor characteristic of the system.[7] At T_B, the above equation requires

$$\frac{1}{T_B} = -\frac{k_B}{\Delta E}\{\ln(2\pi f) + \ln(\tau_0)\} \tag{4}$$

and the values of ΔE can be estimated from the slope of the Arrhénius plot. Figure 7 reveals that the slope of the Arrhénius plot for compound (1) is reduced by pressurization, suggesting the pressure-induced enhancement of ΔE. Figure 8 informs us that the ΔE of compound (1) is enhanced linearly against pressure for $P<5$ kbar, and that, above P =7 kbar, the enhancement relaxes. At around P=10 kbar, the pressure dependence shows a tendency toward saturation. This pressure dependence of ΔE is qualitatively similar to that of T_B. At P=13.1 kbar, the value of ΔE increases up to 1.07 times the initial value, and the relaxation time at T

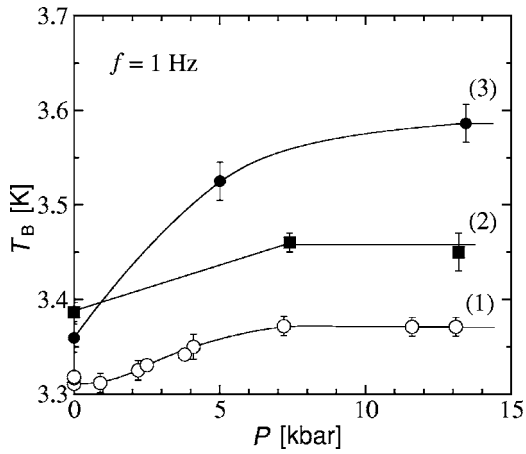

FIG. 6. Pressure dependence of the blocking temperature T_B for f=1 Hz, the lowest frequency in the present experiment, for (1)–(3).

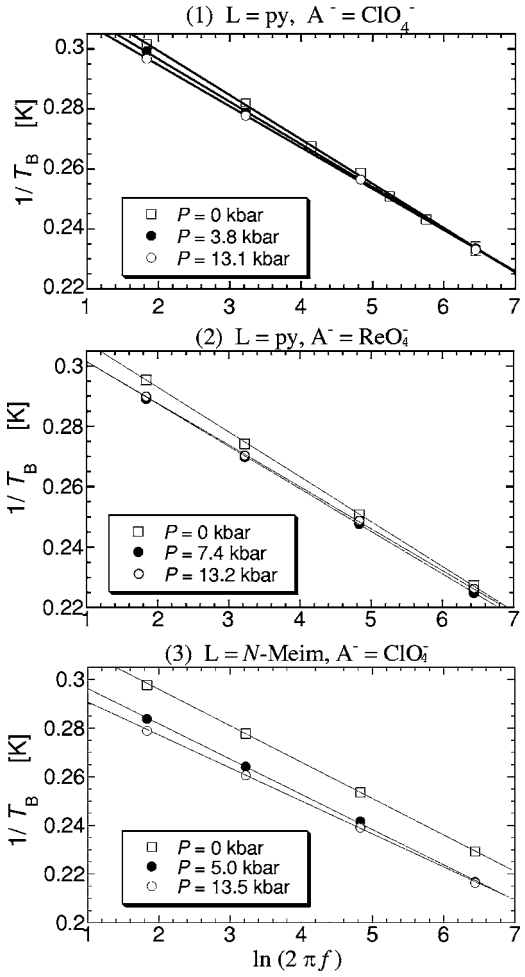

FIG. 7. The Arrhénius plots of the frequency dependence of T_B under various pressures for compounds (1)–(3).

$=1.8$ K, estimated from Eq. (3), is extended from 55 days ($\Delta E/k_B=67.7$ K, $\tau_0=2.2\times10^{-10}$ s) at ambient pressure to 248 days ($\Delta E/k_B=72.7$ K, $\tau_0=6.8\times10^{-11}$ s). The blocking temperature (T_B) which induces the frozen magnetic state increases only slightly, while the lifetime itself is greatly enhanced by pressurization, reflecting the increase in ΔE to a remarkable degree. The drastic increase in τ is worth emphasizing as a desirable effect. Finally, we make an additional remark that the reproducibility of the magnetic properties after releasing the pressure was confirmed via the measurements at ambient pressure once the material was subjected to $P=13.1$ kbar.

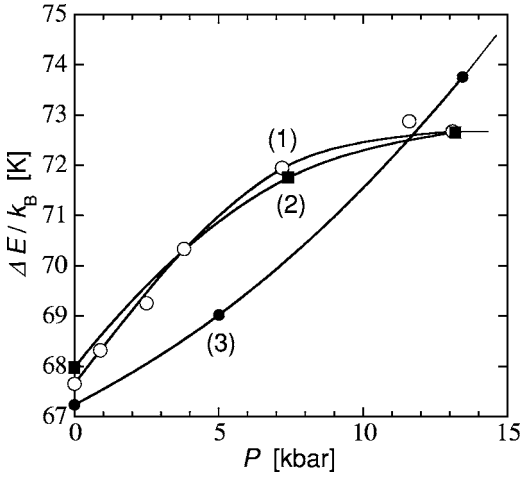

FIG. 8. Pressure dependence of the energy barrier $\Delta E/k_B$ estimated from the slope of the Arrhénius plots for compounds (1)–(3). The solid curves are visual guides.

2. L=py, $A^-=ReO_4^-$

Compound (2) has the same L as compound (1), and its intrachain structure is the same as that of compound (1). As for A^-, ReO_4^- is larger than the ClO_4^- of compound (1), but the one-dimensionality hardly changes, as seen from the data for the minimum nearest interchain intermetallic distance [10.39 Å for compound (1)[7] and 10.30 Å for compound (2)].[8] The measurements for compound (2) were performed at three pressures, $P=0$, 7.4, and 13.2 kbar, and the resulting χ'' data are shown in Fig. 4. It is immediately noticeable that the phenomenon of critical slowing-down of the magnetic moment seen at ambient pressure is also detected at $P=7.4$ and 13.2 kbar, and as a whole, the pressure dependence is similar to that for compound (1). The pressure dependence of T_B at $f=1$ Hz, shown in Fig. 6, reveals that the pressure dependence is also quantitatively similar to that of compound (1), and the maximum magnitude is almost the same as that for compound (1), 0.07 K. Figure 8 indicates that the pressure dependence of the energy barrier ΔE for compound (2), estimated from the slope of the Arrhénius plot (see Fig. 7), is almost consistent with that for compound (1). At $P=13.2$ kbar, the $\tau(T=1.8\ \mathrm{K})$ for compound (2) increases from 94 days ($\Delta E/k_B=68.0$ K, $\tau_0=3.1\times10^{-10}$ s) at ambient pressure to 495 days ($\Delta E/k_B=72.7$ K, $\tau_0=1.2\times10^{-10}$ s). Although the values of the maximum pressure in the experiments for compounds (1) and (2) are very close, it is also interesting that the values for the increase ratio of τ at the most pressurized state are very close, 4.5 for compound (1) and 5.3 for compound (2).

3. L=*N*-Meim, $A^-=ClO_4^-$

Compound (3) has the same counteranion A^- as compound (1), but has a different intrachain attaching ligand $L=N$-Meim on Ni^{II} ion. The ac susceptibility measurements were performed for three pressures, $P=0$, 5.0, and 13.5 kbar. As seen in Fig. 5, the effects of pressure on compound (3), observed through the ac measurements, were qualitatively similar to those on compounds (1) and (2), but it is impressive that the frozen magnetic state at each frequency became more stable with increasing pressure. Figure 6 reveals that the pressure dependence of T_B at $f=1$ Hz for compound (3) is quantitatively different from that of the first two compounds, and the maximum enhancement is 0.23 K [more than three times those for compounds (1) and (2)]. The analyses using the Arrhénius plot shown in Fig. 7 revealed that the magnitude of ΔE for compound (3), estimated from the slope, continued to increase in the considered pressure region, in contrast to compounds (1) and (2), as shown in Fig. 8. At $P=13.5$ kbar, ΔE is enhanced from 67.2 K at

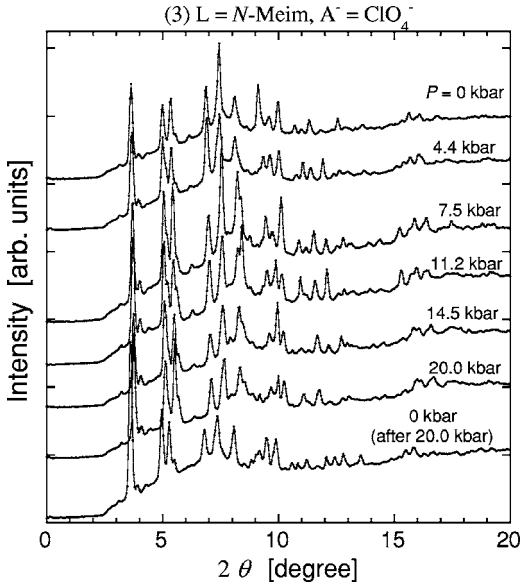

FIG. 9. Powdered x-ray diffraction pattern for compound (3) for pressures up to 20.0 kbar. The measurements were done in the following order: $0 \rightarrow 4.4 \rightarrow 7.5 \rightarrow 11.2 \rightarrow 14.5 \rightarrow 20.0 \rightarrow 0$ kbar.

ambient pressure up to 73.8 K[$=1.10 \times \Delta E(P=0)$], and $\tau(T=1.8\ \mathrm{K})$ is extended from 63 days ($\Delta E/k_B = 67.2$ K, $\tau_0 = 3.2 \times 10^{-10}$ s) at ambient pressure up to 1407 days ($\Delta E/k_B = 73.8$ K, $\tau_0 = 1.8 \times 10^{-10}$ s). The increase ratio of $\tau(T=1.8\ \mathrm{K})$ at $P=13.5$ kbar is 22.3, which is remarkably higher than those for compounds (1) and (2) at around $P = 13$ kbar. It is noteworthy that we succeeded in producing the most effective enhancement of the energy barrier for spin reversal in compound (3).

B. Crystal structural analysis

Figure 9 shows the powdered x-ray diffraction pattern for compound (3) in the pressure region up to 20.0 kbar, and we confirmed that all of the diffraction peaks can be labeled with the $C2/c$ plane index. In a series of pressure experiments, no drastic change in the pattern suggesting any change in the space group was detected. The experiments for compounds (1) and (2) also yielded similar results. Thus, on the assumption that the crystal system does not change in the considered pressure region, we estimated the lattice constants for compounds (1)–(3) at each pressure based on position of some diffraction peaks. The 1D chain of this SCM system runs along the $\langle 101 \rangle$ direction, and the changes in the lattice dimension, the a and c axes, give some information about the change in the intrachain structure. On the other hand, the occurrence of interchain shrinkage may be estimated from the change in the b axis. Figure 10 shows the pressure dependence of the lattice constants for compounds (1)–(3). Here, the data for β are omitted because the change due to pressurization is hardy detected overall in the whole pressure range measured.

As mentioned in the above section, the pressure dependence of ΔE is almost identical for compounds (1) and (2), whereas the pressure dependence of crystallographic parameters a, b, and c differ qualitatively. However, compounds (1) and (2) have a common characteristic, namely that the shrinkage ratio for a is much larger than those for the other axes. This indicates that these SCM chains shrink by distorting the intrachain bonds of the initial state. In contrast, each lattice constant in compound (3) shows consistent behavior under various pressures, suggesting the success of isotropic crystal transformation, and the distance between the metallic ions becomes small, which means that the original coordination environment is maintained during the shrinkage process. Furthermore, it is clear based on the small volume shrinkage in the considered pressure region that the structure of compound (3) is harder than those of the other compounds. Overall, the volume of all compounds continues to decrease in the considered pressure region.

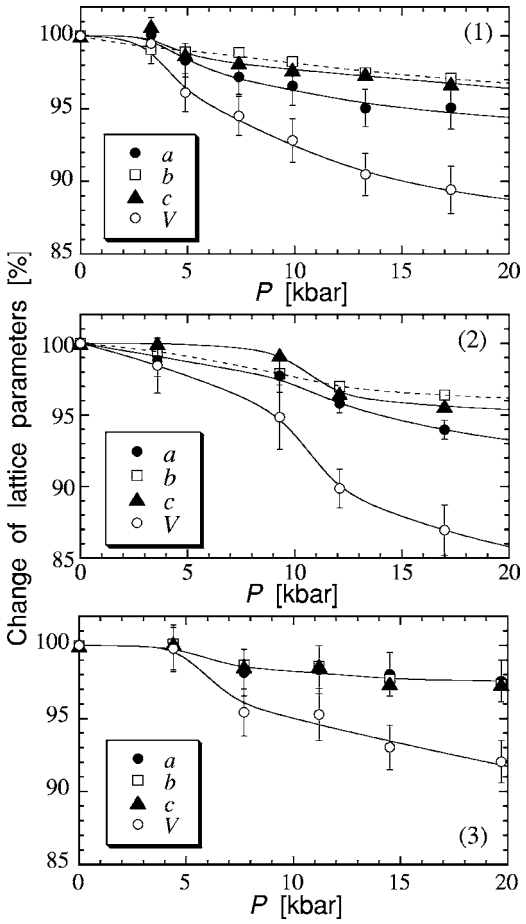

FIG. 10. Pressure dependence of the lattice parameters for compounds (1)–(3). On the assumption that the crystal system does not change in the considered pressure region, the lattice constants at each pressure were estimated based on the positions of some diffraction peaks. The solid and dotted curves are visual guides. The data for β are omitted because changes due to pressurization were hardy detected overall.

Here, we discuss why compound (3) shrinks uniformly, while compounds (1) and (2) shrink in a distorted manner. Considering the packing motif of these compounds, each chain is located with the sliding of a half period along the chain via some counteranions: The Mn^{III}-Mn^{III} dimer of a chain has the closest intermetallic contact with the Ni^{II} ion of

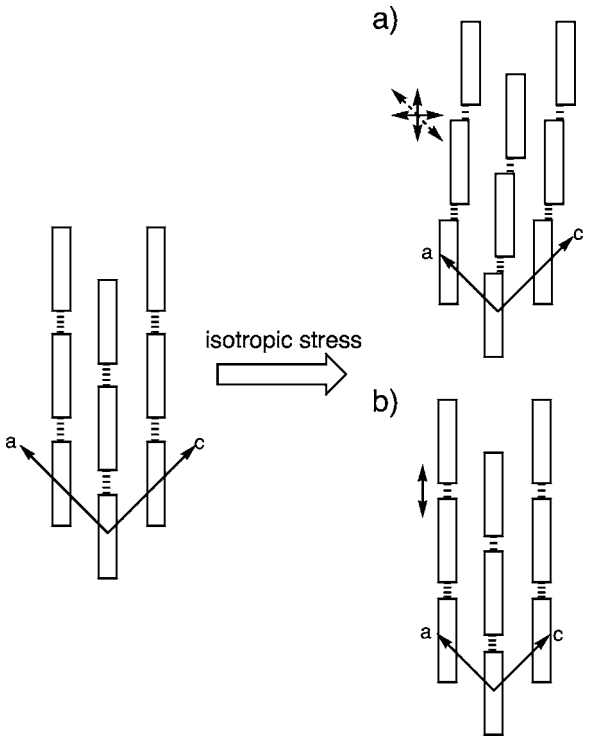

FIG. 11. Schematic representation on presumable structural changes under an isotropic pressure: (a) nonisotropic (distorted) structural change for compounds (1) and (2); (b) isotropic structural change for compound (3). The square and dotted line represent the $S=3$ units of [Mn^{III}-Ni^{II}-Mn^{III}] and Mn-O bonds connecting the $S=3$ units, respectively.

the nearest neighboring chain. When it is recalled that *N*-Meim is bigger than py, it is reasonable to assume that the void space between the interchain $[Mn_2(saltmen)_2]$ dimeric moiety and Ni^{II}-L moiety in compound (3) is smaller than in compounds (1) and (2): i.e., the structure of compound (3) has denser chain structure than those of compounds (1) and (2). Therefore, as for the interchain package, the structure in compound (3) is also the densest among the three. We speculate the following structural transformation. In the chains of compounds (1) and (2), the presence of much void space between the chain permits nonisotropic distortion to the chain-perpendicular direction in addition to the chain-parallel direction during the shrinkage process [Fig. 11(a)], producing the difference between lattice dimensions of the *a* and *c* axes (where chains run on the *ac* plane), whereas the chain of compound (3) can shrink maintaining the initial symmetry against hydrostatic pressurization due to the stable coordination space against external stress. Consequently, in compound (3), the stress can be reduced, directly and merely, by shrinking Mn-O bonds in the $[Mn_2(saltmen)_2]$ dimeric moieties [Fig. 11(b)], allowing an even reduction of the *a* and *c* axes. When we could determine the positions of all atoms by more detailed structural analysis, the above speculative model would be appreciated.

IV. DISCUSSION

The SCM compounds belonging to the $[Mn_2(saltmen)_2Ni(pao)_2(L)_2](A)_2$ family have nice one-dimensionalities due to the existence of effective counteranions A^- evenly located around a chain. Because of the stable counteranion networks, the overall characteristics of these SCMs are also stable. In fact, there appears to be no long-range ordering in the considered pressure region. Furthermore, it has been confirmed through the powdered x-ray diffraction experiments that the crystal systems of the three SCM compounds do not change, and that these structures have enough elasticity to enable them to reconfigure themselves according to the initial crystal structure even after being subjected to pressure as high as 20 kbar.

In all of the three SCM compounds belonging to the $[Mn_2(saltmen)_2Ni(pao)_2(L)_2](A)_2$ family, the pressure-induced stabilization of magnetic relaxation accompanying the enhancement of T_B and ΔE has been observed. Here, the following question must be answered, what enhances ΔE? In this family, the magnitude of ΔE depends on the inter-trimer ferromagnetic interaction J_{trimer} and the negative single-ion anisotropy D.[8,9] The antiferromagnetic interaction of about -20 K between the Mn^{III} and Ni^{II} ions probably has no important influence on the dynamical magnetic properties of the compound in the temperature region below the liquid-helium temperature. The inter-trimer ferromagnetic interaction J_{trimer} has a magnitude of about 1 K in the original state, and the pressure dependence can greatly influence the stability of the energy barrier for spin reversal. Essentially, the orthogonal network for the ferromagnetic correlation may be rather dominantly affected by external stress, as compared to the antiferromagnetic network. In particular, the nonisotropic shrinkage probably results in both the enhancement of ferromagnetic contribution, due to decrease of Mn-O bond length, and partial instability of the orthogonal bonding, due to a change of the Mn-O-Mn angle, and consequently J_{trimer} is not guaranteed to increase to counteract pressurization. The present magnetic and structural experiments revealed the following. The shrinkage distortion seen in compounds (1) and (2) induced a pronounced change in ΔE at small pressures, and finally a state without magnetic sensitivity to pressure was realized. The isotropic shrinkage seen in compound (3), however, made ΔE increase continuously in the considered pressure region. As for the first two compounds, J_{trimer} may have increased during the initial pressurizing because the effect of the decrease in the interatomic distance (Mn-O bonds) overcame that of the slight distortion. But under large stresses such as those above 7 kbar, shrinkage maintaining a distorted minimum energy state occurred, which means that the effective increase in J_{trimer} was not likely [imagine the structural change like Fig. 11(a)]. In the third compound, a continuous increase in J_{trimer} would have been expected as far as the isotropic lattice shrinkage continued [imagine Fig. 11(b)]. On the other hand, the single-ion magnetic anisotropy vector D played the role of locking the direction of the magnetic moment along the D vector, and we have to consider the change against pressure. However, it is necessary for the evaluation of D to decide the coordination environment around the Mn^{III} ions under pressure, but at the present stage we cannot perform such an evaluation. For reference, in Mn_{12}-acetate ($Mn_{12}O_{12}(O_2CCH_3)_{16}(H_2O)_4$) (Ref. 11) as an SMM compound, the increase in $|D|$ at 10 kbar is estimated to be 3.5%. In the case of an SCM system, which is a 1D

network SMMs, the above value cannot be directly referred due to the 1D structural restriction, but the enhancement of ΔE, which was as large as 10% in compound (3), must depend on a distinct increase in ferromagnetic interaction.

Finally, we found in this study that the artificial control of materials using pressure can be an effective and attractive research method, whereas steering the characteristics of the materials in a specific direction is very difficult. In the case of the present SCM system, although it is difficult to markedly enhance the anisotropy connected with the local distortion of the structure, it may be a reasonable approach to try to increase the ferromagnetic intertrimer interaction by inducing the isotropic lattice shrinkage. Thus for compound (3), we are planning an experiment using a DAC in the pressure region above 15 kbar, expecting the further enhancement of ΔE.

V. CONCLUSION

We investigated the effects of pressure on the heterometallic single-chain magnet $[Mn_2(saltmen)_2Ni(pao)_2(L)_2](A)_2$ with repeating units of the Mn^{III}-Ni^{II}-Mn^{III} trimer through ac susceptibility measurements up to 13.5 kbar and powdered crystal structural analyses up to 20.0 kbar. Experiments have been performed for three compounds with different pairs of intrachain attaching ligand (L) and interchain counteranion (A^-). In all compounds, it has been experimentally confirmed that the artificial increase of the ferromagnetic interaction due to external pressure greatly enhances the energy barrier, blocking temperature and relaxation time. This pressure dependence clearly depends on the kind of L involved. While the two SCM compounds which undergo distortion shrinkage under pressure [(1) ($L=$pyridine(py), $A^-=ClO_4^-$) and (2) ($L=py, A^-=ReO_4^-$)] tend to have no magnetic response to high pressures of around 10 kbar, the SCM compound which displays isotropic shrinkage [(3) ($L=N$-methylimidazole (N-Meim), $A^-=ClO_4^-$] exhibits a continuous increase in magnetism in the considered pressure region. Among the three compounds, the most effective control of the material was realized for compound (3), which forms the densest intrachain and interchain structures of the three. At $P=13.5$ kbar, we observed a 10% increase of the energy barrier in compound (3), and a drastic 22-fold extension of the relaxation time at $T=1.8$ K. Through this study, we recognized that the rational boosting of the ferromagnetic interaction by uniform shrinkage is a promising strategy for the effective enhancement of the energy barrier in SCMs.

ACKNOWLEDGMENTS

This work was supported by the PRESTO and CREST projects, the Japan Science and Technology Agency (JST), and a Grant-in-Aid from the Ministry of Education, Culture, Sports, Science and Technology of Japan.

*Email address: mitoh@elcs.kyutech.ac.jp

[1] R. Sessoli, H.-L. Tsai, A. Schake, S. Wang, J. Vincent, K. Folting, D. Gatteschi, G. Christou, and D. Hendrikson, J. Am. Chem. Soc. **115**, 1804 (1993); R. Sessoli, D. Gatteschi, A. Caneschi, and M. A. Novak, Nature (London) **365**, 141 (1993); D. Gatteschi and R. Sessoli, Angew. Chem., Int. Ed. **42**, 1 (2003).

[2] C. Delfs, D. Gatteschi, L. Pardi, R. Sessoli, K. Wieghardt, and D. Hanke, Inorg. Chem. **32**, 3099 (1993); A. Barra, P. Debrunner, D. Gatteschi, C. Schulz, and R. Sessoli, Europhys. Lett. **35**, 133 (1996).

[3] L. Onsager, Phys. Rev. **65**, 117 (1944).

[4] R. J. Glauber, J. Math. Phys. **4**, 294 (1963).

[5] A. Caneschi, D. Gatteschi, N. Lalioti, C. Sangregorio, R. Sessoli, G. Venturi, A. Vindigni, A. Rettori, M. G. Pini, and M. A. Novak, Angew. Chem., Int. Ed. **40**, 1760 (2001).

[6] A. Caneschi, D. Gatteschi, N. Lalioti, C. Sangregorio, R. Sessoli, G. Venturi, A. Vindigni, A. Rettori, M. G. Pini, and M. A. Novak, Europhys. Lett. **58**, 771 (2002).

[7] R. Clérac, H. Miyasaka, M. Yamashita, and C. Coulon, J. Am. Chem. Soc. **124**, 12837 (2002).

[8] H. Miyasaka, R. Clérac, K. Mizushima, K. Sugiura, M. Yamashita, W. Wernsdorfer, and C. Coulon, Inorg. Chem. **42**, 8203 (2003).

[9] C. Coulon, R. Clérac, L. Lecren, W. Wernsdorfer, and H. Miyasaka, Phys. Rev. B **69**, 132408 (2004).

[10] H. Miyasaka, T. Nezu, K. Sugimoto, K. Sugiura, M. Yamashita, and R. Clérac, Chem. Eur. J. **11**, 1592 (2005).

[11] Y. Murata, K. Takeda, T. Sekine, M. Ogata, and K. Awaga, J. Phys. Soc. Jpn. **67**, 3014 (1998).

[12] H. Miyasaka, R. Clérac, T. Ishii, H.-C. Chang, S. Kitagawa, and M. Yamashita, J. Chem. Soc. Dalton Trans. , 1528 (2002).

[13] A. Eiling and J. S. Schilling, J. Phys. F: Met. Phys. **11**, 623 (1981).

[14] A. Fujiwara, K. Ishii, T. Watanuki, H. Suematsu, H. Nakao, K. Ohwada, Y. Fujii, Y. Murakami, T. Mori, H. Kawada, T. Kikegara, O. Shimomura, T. Matsubara, H. Hanabusa, S. Daicho, S. Kitamura, and C. Katayama, J. Appl. Crystallogr. **33**, 1241 (2000).

[15] G. J. Piermarini, S. Block, J. D. Barnett, and R. A. Forman, J. Appl. Phys. **46**, 2774 (1975).